THE JOURNAL OF PHYSICAL CHEMISTRY A

Article

Cite This: J. Phys. Chem. A 2019, 123, 218−229

pubs.acs.org/JPCA

An Extended Computational Study of Criegee Intermediate−Alcohol Reactions

Published as part of The Journal of Physical Chemistry virtual special issue "Young Scientists".

Nathan A. I. Watson, Joshua A. Black,† Thomas M. Stonelake, Peter J. Knowles, and Joseph M. Beames*

School of Chemistry, Cardiff University, Main Building, Park Pl, Cardiff CF10 3AT, United Kingdom

Supporting Information

ABSTRACT: High-level ab initio calculations (DF-LCCSD(T)-F12a//B3LYP/aug-cc-pVTZ) are performed on a range of stabilized Criegee intermediate (sCI)−alcohol reactions, computing reaction coordinate energies, leading to the formation of α-alkoxyalkyl hydroperoxides (AAAHs). These potential energy surfaces are used to model bimolecular reaction kinetics over a range of temperatures. The calculations performed in this work reproduce the complicated temperature-dependent reaction rates of CH_2OO and $(CH_3)_2COO$ with methanol, which have previously been experimentally determined. This methodology is then extended to compute reaction rates of 22 different Criegee intermediates with methanol, including several intermediates derived from isoprene ozonolysis. In some cases, sCI−alcohol reaction rates approach those of sCI−$(H_2O)_2$. This suggests that in regions with elevated alcohol concentrations, such as urban Brazil, these reactions may generate significant quantities of AAAHs and may begin to compete with sCI reactions with other trace tropospheric pollutants such as SO_2. This work also demonstrates the ability of alcohols to catalyze the 1,4-H transfer unimolecular decomposition of α-methyl substituted sCIs.

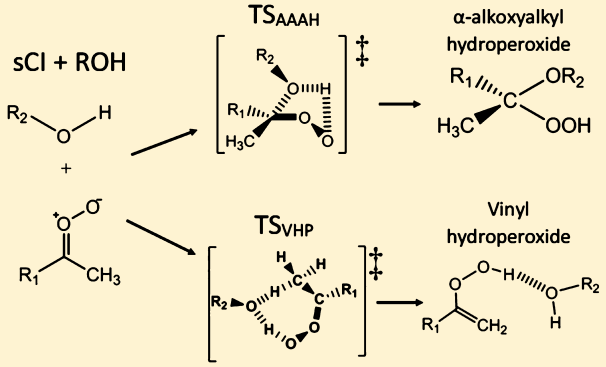

1. INTRODUCTION

Criegee Intermediates (CIs), also known as carbonyl oxides, are atmospheric intermediates that are a significant non-photolytic source of tropospheric hydroxyl (OH) radicals, often considered as atmospheric "detergents".[1] In the laboratory, Criegee intermediates are produced through several different reactions mechanisms including the UV photolysis of iodoalkanes in the presence of oxygen, reaction between oxygen and dimethyl sulfoxide radicals, and the 1,3-cycloaddition of ozone to alkenes (Scheme 1).[2−4]

Scheme 1. General Alkene Ozonolysis Schematic

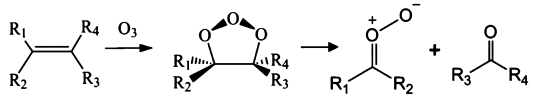

Scheme 1 (shown above) is a prevalent loss mechanism for tropospheric alkenes, and it is the most significant source of tropospheric Criegee intermediates. Alkene ozonolysis produces carbonyl oxides with significant internal energy (e.g., 2,3-dimethylbutane ozonolysis produces an excess energy of 200−250 kJ mol^{-1}).[5] This internal energy leads to 37%−50% of the total tropospheric yield of carbonyl oxides, undergoing rapid unimolecular decomposition.[5−15] The remaining fraction are collisionally stabilized and eventually lost through bimolecular reactions, UV photolysis, or slower thermal decomposition.[5,6,12,14,15] There has been a significant body of work investigating bimolecular reaction mechanisms and rates of stabilized Criegee intermediates (sCIs) with trace atmospheric constituents, focusing on the fate of tropospheric sCIs and the role of these reactions in influencing the tropospheric HO_x budget, and in the formation of atmospheric aerosols.

Alkene tropospheric abundances are strongly localized: in urban areas, short-chain alkenes tend to be the most prevalent, whereas in forested regions foliar emissions mean that terpenes and sesquiterpenes become predominant. sCIs may differ in atmospheric fate based on their chemical and electronic structure, as indicated by the greater rate of unimolecular decomposition shown by $(CH_3)_2COO$ (k_{decay} = 11.6 s^{-1}) than CH_2OO (k_{decay} = 305 s^{-1}).[16,17] These sCIs also differ in reaction rates with atmospheric species: CH_2OO reacts faster with $(H_2O)_2$ than SO_2, whereas the reverse is true for $(CH_3)_2COO$.[3,18,19] There is a growing body of evidence also suggesting that water droplets can also alter sCI reactions, where the surface chemistry of the sCI is significantly different

Received: September 25, 2018
Revised: November 30, 2018
Published: December 3, 2018

DOI: 10.1021/acs.jpca.8b09349
J. Phys. Chem. A 2019, 123, 218−229

to gaseous sCI reactivity.[20−27] Additionally, a comparative computational study of the sCI−H_2O reaction shows that heteroatom substitution of the H_2O oxygen with other group 16 elements alters the reaction barriers and reaction rates.[28] This is also evidenced in sCI reactions with SiH_4 and with CH_4.[20] Heteroatom tuning of reaction rates has also been demonstrated for substitution of the sCI oxygens or carbon, for example, the case of thioformaldehyde *S*-sulfide formation in place of the carbonyl oxide.[29,30]

Gaseous bimolecular reactions of sCIs with alcohols are another example of a class of chemical reactions that lead to a net removal of atmospheric sCIs.[31] Atmospheric alcohols (predominantly methanol, ethanol, and isopropyl alcohol) arise from both biogenic and anthropogenic sources and have appreciable tropospheric concentrations, varying from ca. 1 ppbv in oceanic regions to ca. 10 ppbv in urban areas.[17−19] In urban environments, where biofuels such as methanol and ethanol are heavily utilized to power both personal and industrial automobiles, local tropospheric alcohol concentrations are substantially increased.[32−36] For example, in Brazil, where the government subsidizes biofuel use as a more environmentally friendly alternative to fossil fuels, many cities exhibit elevated tropospheric alcohol levels.[37] In heavily populated regions of Brazil like São Paulo, Rio de Janeiro, or Porto Allegro concentrations of alcohols can reach 400 ppbv, increasing to in excess of 450 ppbv of ethanol in areas where urban and industrial emissions are combined.[32−36]

Reactions between gaseous alcohols and Criegee intermediates lead to the production of atmospheric α-alkoxyalkyl hydroperoxides (AAAHs; Scheme 2), which can in turn be stabilized and are subsequently photolyzed or decompose through reactions with other reactive species such as hydroxyl radicals.[8,38−40]

Scheme 2. Formation of AAAHs from Stabilized Criegee Intermediates

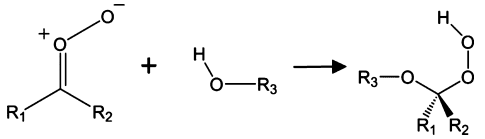

In 1996, Moorgat and co-workers began to investigate sCI−alcohol reactions by using Criegee intermediate precursors ethene and ozone to synthesize methoxymethyl hydroperoxides.[41] In 2003, C13 sCIs were reacted with gaseous methanol and isopropyl alcohol to compare reactivity with other small intermediates.[42] More recently, direct detection of Criegee intermediates facilitated the elucidation of bimolecular reaction rates for formaldehyde oxide with methanol, ethanol, and isopropyl alcohol as well as those for both *anti*-CH_3CHOO and $(CH_3)_2COO$ with methanol.[39,40,43] Orr-Ewing and co-workers also demonstrated that this class of reactions may be an important source of AAAHs, occurring specifically around tropical rainforests (~24 Gg yr^{-1}) as well as boreal forests (~3 Gg yr^{-1}) and temperate forests (~2 Gg yr^{-1}).[39] Their work also demonstrated a negative temperature dependence for the reaction of CH_2OO with methanol or ethanol, whereas the reaction of $(CH_3)_2COO$ with methanol has mixed temperature dependence, with a point of inversion at ca. 285 K.[39]

This work provides a more comprehensive computational study of sCI−alcohol reactions, assembling and analyzing reaction pathways for a series of different sCIs with alcohols. These data are compiled in a manner similar to those generated for sCI reactions with CO, CH_4, H_2, and H_2O, identifying trends in reactivity as a function of both sCI substituents and alcohol size.[20−22,44,45] Reaction rates, computed as a function of temperature, are benchmarked against the recent experimental data, ensuring the qualitative accuracy of the potential energy surfaces. Reaction rates are used to evaluate the potential significance of these reactions under typical tropospheric conditions.

2. COMPUTATIONAL METHODS

All stationary points on the reaction pathways explored in this study are fully optimized using density functional theory (DFT), employing the hybrid B3LYP functional and the Dunning correlation-consistent aug-cc-pVTZ basis set (B3LYP/aug-cc-pVTZ). In a few limited cases, as noted in the main text, the basis set was reduced to aug-cc-pVDZ.[46−49] The nature of each stationary point, either minimum or transition state, is verified through harmonic vibrational frequency calculations, at the same level of theory as the geometric optimization. In addition, each transition state is mapped to the minima it links through the use of intrinsic reaction coordinate (IRC) calculations, utilizing a steepest descent algorithm.[50,51] All geometry optimizations, vibrational frequency calculations, and IRCs are undertaken in the Gaussian09 computational chemistry suite.[52]

An explicitly correlated, local density fitted coupled cluster approach (DF-LCCSD(T)-F12a/aug-cc-pVTZ) is used to refine the molecular energies of each of the stationary points computed above, performed in the MOLPRO computational package.[53,54] Energies are zero-point corrected using the density functional harmonic vibrational frequencies. As demonstrated herein, these methodologies provide a good combination of energetic accuracy and low computational cost, affording the application of these methods to a range of sCI sizes and reactions.

Rate constants are calculated using conventional transition-state theory. The *Kinetic and Statistical Thermodynamical Package* (KiSThelP)[55] software is used to compute each rate constant k_{total} [eqn 1]; utilizing the product of the K_{eq} equilibrium constant between reactants and prereaction complex [eqn 2] and k_2 the unimolecular rate constant [eqn 3]:

$$k_{total} = \sum (K_{eq} \cdot k_2) \tag{1}$$

$$K_{eq} = \frac{RT}{p_0} e^{-(G_{PRC}-(G_{CI}+G_{ROH}))/RT} \tag{2}$$

$$k_2 = \kappa \frac{k_B T}{h} e^{-(G_{TS}-G_{PRC})/RT} \tag{3}$$

This approach is adapted from previous work on similar systems,[45,56] where κ is the tunneling constant; k_B is Boltzmann constant; T is temperature; h is Planck's constant; R is the gas constant; p_0 is the pressure of the system; G_{TS}, G_{PRC}, G_{CI}, and G_{ROH} are the molar Gibbs free energies for transition state, prereaction complex, Criegee intermediate, and alcohol. Standard temperature and pressure are used, unless stated otherwise.

DOI: 10.1021/acs.jpca.8b09349
J. Phys. Chem. A 2019, 123, 218−229

The tunneling factor (κ) is calculated using an asymmetric Eckart function, which is a non-ab initio method that takes into account the barrier width between the reactants and the product.[55] With eqs 4−(10) the Eckart function is calculated from the probability of transmission through the one-dimensional energy barrier $p(E)$:

$$p(E) = 1 - \left[\frac{\cosh[2\pi(\alpha - \beta)] + \cosh[2\pi\delta]}{\cosh[2\pi(\alpha + \beta)] + \cosh[2\pi\delta]}\right] \quad (4)$$

$$\alpha = \frac{1}{2\sqrt{C}}\sqrt{E} \quad (5)$$

$$\beta = \frac{1}{2\sqrt{C}}\sqrt{E - A} \quad (6)$$

$$\delta = \frac{1}{2\sqrt{C}}\sqrt{B - C} \quad (7)$$

$$A = \Delta H_f^{\ddagger,0K} - \Delta H_r^{\ddagger,0K} \quad (8)$$

$$B = \sqrt{\Delta H_f^{\ddagger,0K}} - \sqrt{\Delta H_r^{\ddagger,0K}} \quad (9)$$

$$C = (h\cdot \mathrm{im}(\nu^{\ddagger}))^2\left[\frac{B^3}{A^2 - B^2}\right]^2 \quad (10)$$

The three factors that are used to determine the energy barrier $p(E)$ are the forward and reverse zero-point corrected energy barriers $\Delta H_f^{\ddagger,0K}$ and $\Delta H_r^{\ddagger,0K}$, respectively, and the imaginary frequency of associated transition state describing the reaction coordinate $\nu^{\ddagger}$. The Eckart tunneling correction factor (κ) can then be calculated from

$$\kappa = \frac{e^{\Delta H_f^{\ddagger,0K}}}{k_b T}\int_0^{\infty} p(E)e^{-E/k_b T}\mathrm{d}E \quad (11)$$

Kinetic and Statistical Thermodynamical Package (KiSThelP) uses a 15-point Gauss−Laguerre integration to evaluate eq 11. This methodology has previously been used to estimate the intramolecular tunneling contributions of Criegee intermediate reactions, in addition to many other bimolecular reactions in which proton tunneling occurs.[45,58−61] This technique has also been verified herein, through comparison with semiclassical on-the-fly instanton methods.

Direct comparisons between the Criegee intermediate reaction rates generated in this study, and other atmospheric bimolecular reaction rates, are facilitated by the computation of coreactant concentration-dependent rate constants (k_{eff}), where[57]

$$k_{eff} = k_{total}[\mathrm{coreactant}] \quad (12)$$

3. RESULTS

This study investigates the reaction pathways and reaction rates of the most tropospherically abundant alcohols, namely, methanol (MeOH or CH_3OH), ethanol (EtOH, C_2H_5OH), and isopropyl alcohol (iPrOH, $(CH_3)_2CHOH$) with a range of different sCIs shown in Figure 1.

The sCIs investigated in this study are chosen for two purposes. First, many of the sCIs (**1**−**22**) are generated in the ozonolysis of tropospherically abundant alkenes; for example, the smaller sCIs (**1**−**4**) are formed from the ozonolysis of ethene, propene, and butene that are typically anthropogenic emissions and are abundant in polluted environments.[62] sCI−Alcohol (**1**−**4**) reaction kinetics have also been determined experimentally and are used to benchmark our methodology. Several of the larger sCIs (**13**−**20**) are generated from the ozonolysis of isoprene, which is the most globally abundant alkene, arising predominantly from biogenic foliar emissions, in forested, pristine environments.[63]

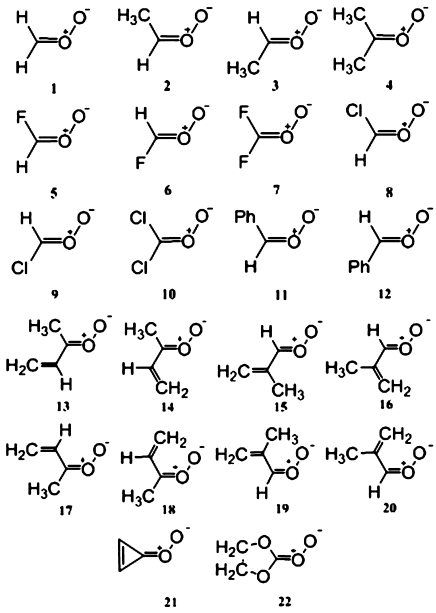

Figure 1. Structures of stabilized Criegee intermediates computed herein. In each case, reaction rates with methanol are evaluated.

Second, a subset of the sCIs are chosen for which the carbonyl oxide substituents significantly modify the electronic character of the carbonyl oxide moiety. It is well-understood that the Criegee intermediates exhibit mixed biradical and zwitterionic character, with the zwitterionic component dominant. However, the degree of zwitterionic character can be tuned somewhat by modifying these carbonyl oxide substituents, for example, by extending the degree of carbonyl oxide (hyper)conjugation (**11**−**20**) or by substitution with electronegative species such as halogens (**5**−**10**, **22**).[21,22,45,64−67] The degree of zwitterionic character can be approximated by the ratio between the R_{OO} and R_{CO} bond lengths (q), where a larger ratio is indicative of more double-bond character in the C−O bond and, thus, the sCI being more zwitterionic in nature.

Several typical sCI−alcohol reaction pathways are illustrated in Figure 2, for the R_1CH_3COO + R_2OH reaction. The first channel, common to all sCI−alcohol reactions, leads to the formation of α-alkoxyalkyl hydroperoxides (AAAH), as previously reported, via a prereaction complex and low-energy transition state.[39,40,43] The prereaction complex is stabilized by a hydrogen-bonding interaction between alcohol hydrogen and the carbonyl oxide terminal oxygen. After complexation, the reactants are positioned for the insertion of the carbonyl oxide into the alcohol O−H bond.

In cases where the sCI has an α-methyl group, the reaction can also proceed through a second competitive channel, in which the alcohol catalyzes the production of a vinyl hydroperoxide (VHP), ultimately leading to the unimolecular decomposition of the sCI. This alcohol-catalyzed reaction is analogous to those previously demonstrated for water−sCI reactions.[22] In most cases, each sCI−alcohol reaction exhibits

DOI: 10.1021/acs.jpca.8b09349
J. Phys. Chem. A 2019, 123, 218−229

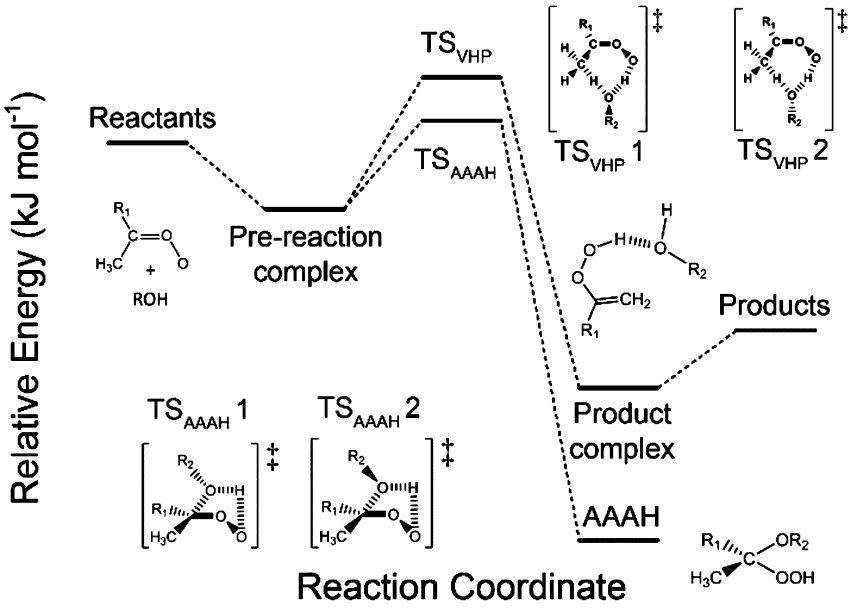

Figure 2. Illustrative potential energy surfaces of possible reaction channels between stabilized Criegee intermediates and alcohols. In most cases there are multiple reaction channels for each set of reactants. The VHP channel is only accessible if the sCI has an α-methyl group.

Table 1. Criegee Intermediate Number (sCI); Alcohol (ROH); Ratio between OO and CO Bond Lengths on the Carbonyl Oxide Moiety (q); Zero-Point Corrected Energies of Prereaction Complex (ΔZPE_{PRC}) and Lowest Transition State (ΔZPE_{TS}); Total Rate Constant Per Channel [$k_{total} = \sum(K_{eq} \cdot k_2)$]; Contribution of Tunneling to Channel [$\kappa_{contr} = \sum(\Gamma \times \kappa)$][a]

sCI	ROH	q	ΔZPE_{PRC} (kJ mol^{-1})	ΔZPE_{TS} (kJ mol^{-1})	k_{total} (cm^3 molec^{-1} s^{-1})	κ_{contr}
1	MeOH	1.078	−28.15	−3.81	1.17×10^{-14}	1.10
	EtOH		−28.65	−7.42	6.17×10^{-14}	1.09
	iPrOH		−28.55	−4.51	1.21×10^{-14}	1.08
2	MeOH	1.084	−29.41	10.04	1.82×10^{-17}	1.17
			−29.41	**27.19**	***1.09 × 10^{-18}***	**25.32**
3	MeOH	1.093	−35.13	−17.73	2.09×10^{-12}	1.16
4	MeOH	1.091	−34.42	1.21	5.63×10^{-16}	1.36
			−34.42	**25.32**	***5.81 × 10^{-18}***	**37.32**
5	MeOH	1.113	−30.42	−15.16	7.62×10^{-13}	1.07
6	MeOH	1.136	−38.52	−32.22	8.66×10^{-10}	1.02
7	MeOH	1.164	−41.27	−40.51	1.96×10^{-8} [b]	1.00
8	MeOH	1.082	−26.80	10.09	1.10×10^{-17}	1.13
9	MeOH	1.104	−35.45	−23.11	6.50×10^{-12}	1.09
10	MeOH	1.093	−27.28	−3.60	2.40×10^{-15}	1.12
11	MeOH	1.075	−22.92	10.09	4.01×10^{-17}	1.36
	EtOH		−21.30	7.45	9.74×10^{-17}	1.31
	iPrOH		−20.83	6.16	7.51×10^{-17}	1.29
12	MeOH	1.084	−31.32	−17.43	1.72×10^{-12}	1.54
	EtOH		−32.42	−21.01	6.51×10^{-12}	1.53
	iPrOH		−33.25	−20.84	2.48×10^{-12}	1.63
13	MeOH	1.065	−24.65	14.66	4.04×10^{-18}	2.14
			−24.65	**36.41**	***4.04 × 10^{-20}***	**46.83**
14	MeOH	1.075	−25.18	7.31	3.66×10^{-17}	1.85
			−25.18	**30.82**	***2.61 × 10^{-19}***	**35.66**
15	MeOH	1.076	−33.16	−9.96	1.61×10^{-13}	1.75
16	MeOH	1.079	−28.19	−15.88	5.10×10^{-13}	1.39
17	MeOH	1.070	−31.88	0.79	1.19×10^{-15}	2.14
18	MeOH	1.069	−22.75	8.44	3.95×10^{-17}	1.55
19	MeOH	1.078	−30.57	3.55	3.75×10^{-16}	1.37
20	MeOH	1.065	−20.69	13.42	4.81×10^{-18}	1.28
21	MeOH	1.186	−57.50	−30.31	3.59×10^{-10} [b]	1.49
22	MeOH	1.174	−54.01	−44.31	4.20×10^{-8} [b]	1.40

[a] Γ is branching ratio; VHP channels in bold and italic fonts. [b] Exceeds the gas collision limit found in Supporting Information Table S2.

DOI: 10.1021/acs.jpca.8b09349
J. Phys. Chem. A 2019, 123, 218−229

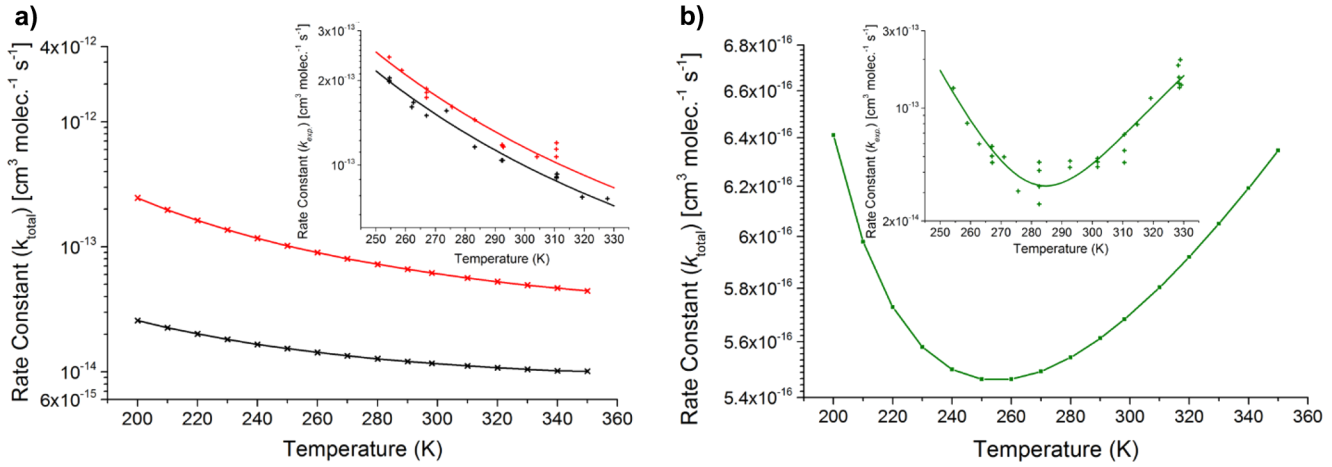

Figure 3. Theoretical temperature dependence of sCI−alcohol reactions: CH_2OO + MeOH (black) and CH_2OO + EtOH (red) (a); $(CH_3)_2COO$ + MeOH (green) (b). (insets) Experimental temperature dependences, taken from the work of Orr-Ewing and co-workers (∼10 Torr). It is worth noting that the computed values are at standard pressure. Figures S1 and S2 show analogous plots in which the computed rate constants are generated at p = 9.99 Torr.

multiple transition states, distinguished by the orientation of the alcohol relative to the sCI. Therefore, the total reaction rate is computed as the sum of individual reaction rates for each transition state. The number of transition states typically increases as the geometric size and complexity of the sCI−alcohol system increases. Table 1, below, displays data computed using the methodologies outlined in Section 2, for all the sCI−alcohol reactions investigated in this work.

4. DISCUSSION

I. Effect of Alcohol Substitution. The reactions of CH_2OO with methanol (MeOH), ethanol (EtOH), and isopropyl alcohol (iPrOH) show little difference in prereaction complex energy but exhibit slight differences in transition-state energies. The lowest-energy transition state, in each case, is lower than the energy of the reactants. The reaction with methanol displays the highest barrier followed by isopropyl alcohol and then ethanol. These relative barrier heights are reflected in the computed rate constants for the reactions of CH_2OO with methanol, isopropyl alcohol, and ethanol being 1.17×10^{-14}, 1.21×10^{-14}, and 6.17×10^{-14} cm^3 molecule^{-1} s^{-1}, respectively. These values are in qualitatively good agreement with experimentally determined rate constants, generated using flash photolysis techniques (1.4×10^{-13}, 1.9×10^{-13}, 2.3×10^{-13} cm^3 molecule^{-1} s^{-1} at 295 K, 90 Torr) and match the trend in reactivities.[40] These values are also in good agreement with those reported by Orr-Ewing and co-workers, for the reactions of CH_2OO with MeOH and EtOH of 1.04×10^{-13} and 1.16×10^{-13} cm^3 molecules^{-1} s^{-1} (at 293 K, 9.99 Torr).[39] It is worth noting that the experimental values are reported at nonstandard temperatures and pressures. Because of multiple transition states, CH_2OO reacts faster with iPrOH than MeOH, in line with experimental results, demonstrating the necessity of exploring more than a single, or lowest-energy, reaction pathway when modeling sCI chemistries.

The computational methodologies used herein are further benchmarked against the temperature dependences reported for CH_2OO + MeOH, CH_2OO + EtOH, and $(CH_3)_2COO$ + MeOH by Orr-Ewing and co-workers. Both CH_2OO reactions exhibit a negative temperature dependence between 255 and 327.8 K, consistent with a low-energy reaction barrier at 9.99 Torr pressure. However, the reaction of $(CH_3)_2COO$ showed a mixed temperature dependence, with an inflection point at T = 285 K. Figure 3 illustrates the computed temperature dependence of these reactions, which once again show good qualitative agreement with experiment, matching these trends in temperature dependences and giving rise to a mixed temperature dependence for the reaction of $(CH_3)_2COO$ + MeOH. The mixed temperature dependence arises from the dominant TS_{AAAH} 1 having an energy close to the reactants, as well as from multiple transition states contributing to k_{total}. At low temperatures k_{total} is dominated by contributions from TS_{AAAH} 1. As the system temperature increases, beyond the modeled inflection point at T = 255 K, other reaction pathways begin to contribute significantly to the total rate, making k_{total} increase sharply. As observed in Supporting Information Figures S1 and S2, the experimental rate constants for $(CH_3)_2COO$ + MeOH at 9.99 Torr show trends as a function of temperature that are also consistent with computed values at this pressure, and these computed values are mostly within 1 order of magnitude of the experiments. It is also clear that the potential energy surfaces computed in this work provide a good model of sCI reactivity, and that may be used to predict the reactivity and relative reaction rates of sCI−alcohol reactions that have not yet been directly observed experimentally. This is also confirmed by a comparison of the rates and Gibbs free energies in the sensitivity study in Supporting Information Table S1.

As highlighted above, this work demonstrates that alkyl substitution of the alcohol has little impact on k_{total}, particularly compared with carbonyl oxide substitution, which alters the reaction rate by many orders of magnitude (Table 1). This invariance in the rate constant with respect to choice of alcohol is maintained when the sCI is sterically bulky, illustrated by the reaction rates of *syn*/*anti*-PhCHOO, and the relative trend in reactivity is also maintained ($k_{MeOH} < k_{iPrOH} < k_{EtOH}$). Because of the lack of variation in reaction rate as a function of changing alcohol, this study focuses instead on investigating the effect of different carbonyl oxide substituents.

II. The Effect of sCI Conformation on Reaction Rates. Criegee intermediates have been shown to demonstrate remarkably different unimolecular and bimolecular reactivities based upon their conformation. An illustration of this can be found in the case of CH_3CHOO (Figure 4), which has two

DOI: 10.1021/acs.jpca.8b09349
J. Phys. Chem. A 2019, 123, 218−229

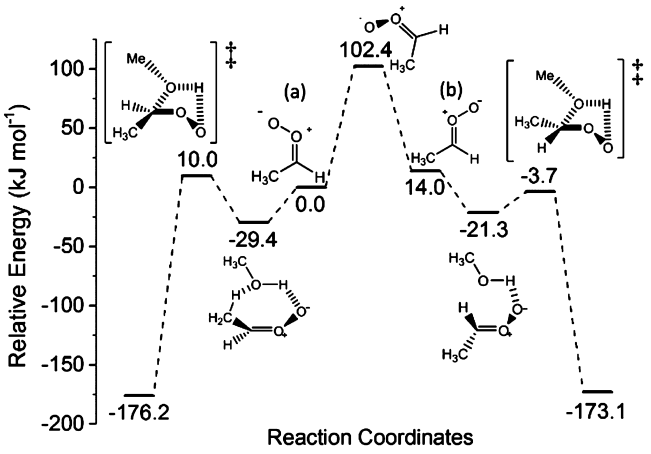

Figure 4. Computed reaction coordinates of *syn*-(CH_3)CHOO (a) and *anti*-(CH_3)CHOO (b) with MeOH.

distinct conformeric forms, namely, *syn*-CH_3CHOO [Figure 4a] and *anti*-CH_3CHOO [Figure 4b]. These conformers have a high barrier to interconversion (~160 kJ mol^{-1}) causing each to have their own distinct bimolecular reaction chemistry, and reaction rates that often differ by orders of magnitude, for example, in the cases of reactions with SO_2, H_2O, and NO_2.[66,68] Figure 4 demonstrates that this chemical distinction is similarly observed in the reaction of CH_3CHOO with methanol.

Figure 4 shows the reaction coordinate of *syn*-CH_3CHOO with methanol exhibits a low-energy prereaction complex (−29.4 kJ mol^{-1}), with a geometry similar to the prereaction complex of $(CH_3)_2COO$ with methanol. The *syn*-CH_3CHOO reaction has a high-energy transition state (+10 kJ mol^{-1}) resulting in a rate constant of k_{total} = 1.93 × 10^{-17} cm^3 $molecule^{-1}$ s^{-1}. The *anti*-CH_3CHOO prereaction complex (see Figure 4) is slightly higher in energy than that of *syn*-CH_3CHOO with geometric parameters more comparable with those of the CH_2OO reaction with methanol. In this case, however, although the prereaction complex is less stable, the reaction barrier is lower in energy (−17.73 kJ mol^{-1}), leading to a bimolecular rate constant 5 orders of magnitude greater than the *syn* conformer (k_{total} = 2.09 × 10^{-12} cm^3 $molecule^{-1}$ s^{-1}). The pressure-adjusted theoretical value for *anti*-CH_3CHOO and methanol (k_{total} (p = 250 Torr, T = 295 K) = 6.38 × 10^{-12} cm^3 $molec^{-1}$ s^{-1}) shows good agreement with the experimentally determined rate constant, recorded by Lin and co-workers of 5 × 10^{-12} cm^3 $molec^{-1}$ s^{-1}, while the *syn*-CH_3CHOO reaction was not recorded.[43]

This trend in reactivity is observed throughout the series of monosubstituted sCIs interrogated in this work (**5**/**6**, **8**/**9**, **11**/**12**, **15**/**19**, and **16**/**20**); the *syn* conformer always exhibits a lower reaction rate constant (k_{total}) compared to its *anti* conformer (Table 2), despite the latter all exhibiting two transition states. The trends in rate constants observed by varying the electronegativity of the substituents for monosubstituted sCIs are also observed for disubstituted sCIs.

The complex isoprene-derived sCIs conformers **15** and **16** are carbonyl oxides with unsaturated alkene groups in the *anti* position. Because of the conjugated nature of the molecules, they have a high barrier to interconversion and display distinct bimolecular reaction rates, such that the sCI(**16**)−alcohol reaction rate is 2 orders of magnitude faster than that of **15**. The same trend is also observed for sCI entries **17** and **18**.

III. Effect of sCI Substitution on the Reaction Rates. Criegee intermediate reactivity can be readily tuned by altering the electronic character of the carbonyl oxide group through substitution. sCIs with greater zwitterionic character typically exhibit greater reaction rate constants, as previously demonstrated for bimolecular sCI reactions with water (monomers and dimers), H_2, and SO_2.[18,20,66,67] This trend is observed throughout the reactions investigated in this study: Figure 5 demonstrates a positive correlation between sCI R_{OO}/R_{CO} bond ratio and the methanol bimolecular reaction rate constant (k_{total}).

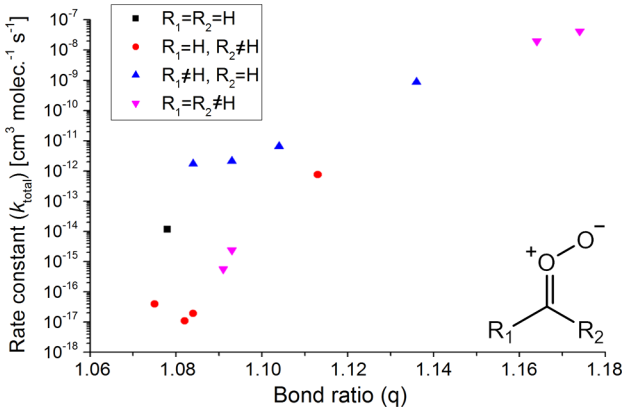

Figure 5. Relationship between ratio between OO and CO bond lengths on the carbonyl oxide moiety (q) and sCI-MeOH rate constant (k_{total}). The plot demonstrates the correlation between (q), an approximate measure of the zwitterionic character of the sCI, and reaction rate.

This trend can be rationalized by considering the relative heights of the reaction barriers, where disubsituted sCIs, substituted with electron-withdrawing groups that increase the zwitterionic character of the intermediate, have lower energy transition states. For example, sCIs such as F_2COO, and Cl_2COO have larger R_{OO}/R_{CO} bond ratios (values) and lower transition states (Table 2), which give rise to reaction rates as in other theoretical analyses.[20,45] The rate constant increases by orders of magnitude ($k_{(CH_3)_2COO} < k_{Cl_2COO} \ll k_{CF_2OO}$), showing that increasing the electronegativity of sCI substituents serves to significantly increase bimolecular rate constants. For CI7, CI21, and CI22 reactions with MeOH,

Table 2. Comparative Tunneling Factors for Unimolecular Uncatalyzed sCI Decomposition

	κ (CI 2)				κ (CI 14)		
T (K)	Wigner function	Eckart function	instanton method DFT (N = 256)	instanton method CCSD(T) (N = 16)	Wigner function	Eckart function	instanton method DFT (N = 128)
160	9.76	2.46 × 10^9	8.12 × 10^8	1.52 × 10^{10}	9.93	9.12 × 10^9	1.08 × 10^9
260	4.32	489.9	284.55	948.4	4.38	690.3	317.53
360	2.73	10.53	13.62	21.35	2.76	11.49	15.93

DOI: 10.1021/acs.jpca.8b09349
J. Phys. Chem. A 2019, 123, 218−229

Table 3. Effective Bimolecular Rate Constants for sCIs with a Range of Tropospheric Constituents[a]

CI	co-reactant	[co-reactant] (molec/cm^3)	k_{total} (cm^3 molecule^{-1} s^{-1})	k_{eff} (th) (s^{-1})	k_{exp} (cm^3 molecule^{-1} s^{-1})	k_{eff} (ex) (s^{-1})	refs
1	MeOH	8.4×10^{11}	1.2×10^{-14}	0.0101	1.4×10^{-13}	0.12	this work, 40
	EtOH	4.3×10^{12}	6.2×10^{-14}	0.27	2.3×10^{-13}	0.099	this work, 40
	iPrOH	1.1×10^{12}	1.2×10^{-14}	0.013	1.9×10^{-13}	0.021	this work, 40
	H_2O	6.2×10^{17}	3.5×10^{-15}	2.2×10^{3}	1.3×10^{-15}	806	67, 78, 79
	$(H_2O)_2$	4.0×10^{14}	2.3×10^{-10}	9.3×10^{4}	7.5×10^{-12}	3.0×10^{3}	18, 67, 78
	O_3	6.0×10^{11}	4.0×10^{-13}	0.24	6.7×10^{-14}	0.040	80−82
	SO_2	8.7×10^{10}	5.1×10^{-10}	44.4	3.9×10^{-11}	3.4	66, 83, 84
	CO	5.1×10^{13}	2.0×10^{-21}	1.0×10^{-7}	unknown	unknown	43, 66
	NO_2	7.0×10^{14}	4.4×10^{-12}	3.1×10^{3}	1.5×10^{-12}	1.1×10^{3}	66, 85
	CO_2	1.0×10^{16}	3.5×10^{-19}	3.5×10^{-3}	$<10^{-17}$	<0.2	57, 86
	HNO_3	1.1×10^{11}	5.1×10^{-10}	57	5.4×10^{-10}	60	87−89
	HCOOH	3.1×10^{11}	1.0×10^{-10}	31	1.1×10^{-10}	2.7	90, 91
	CH_3COOH	3.9×10^{10}	unknown	unknown	1.3×10^{-10}	16	90, 92
	CF_3COOH	2.9×10^{4}	1.9×10^{-10} [b]	5.4×10^{-6} [b]	3.4×10^{-10}	9.7×10^{-6}	93, 94
	HCl	3.2×10^{10}	4.1×10^{-11}	1.3	4.6×10^{-11}	1.5	88, 95
2	MeOH	8.4×10^{11}	1.9×10^{-17}	1.6×10^{-5}	unknown	unknown	this work
	$(H_2O)_2$	4.0×10^{14}	1.4×10^{-12}	278	unknown	unknown	18, 67
	SO_2	8.7×10^{10}	unknown	unknown	2.4×10^{-11}	2.1	68
	[thermal decomposition]					166	79
	HCOOH	3.1×10^{11}	unknown	unknown	2.5×10^{-10}	78	90
	CH_3COOH	3.9×10^{10}	unknown	unknown	1.7×10^{-10}	6.7	90
3	MeOH	8.4×10^{11}	2.1×10^{-12}	1.8	5×10^{-12}	4.2	this work, 43
	$(H_2O)_2$	4.0×10^{14}	1.1×10^{-09}	4.2×10^{5}	4.4×10^{-11}	1.8×10^{4}	18, 67, 96
	SO_2	8.7×10^{10}	unknown	unknown	6.7×10^{-11}	5.8	68
	HCOOH	3.1×10^{11}	unknown	unknown	5.0×10^{-10}	160	90
	CH_3COOH	3.9×10^{10}	unknown	unknown	2.5×10^{-10}	9.9	90
4	MeOH	8.4×10^{11}	5.7×10^{-16}	4.7×10^{-4}	4.3×10^{-14}	0.036	this work, 39
	$(H_2O)_2$	4.0×10^{14}	7.0×10^{-13}	280	$<1.3 \times 10^{-13}$	<52	18, 67
	SO_2	8.7×10^{10}	4.0×10^{-10}	34	1.3×10^{-11}	1.1	18, 97
	HCOOH	3.1×10^{11}	unknown	unknown	3.1×10^{-10}	97	98
	CH_3COOH	3.9×10^{10}	unknown	unknown	3.1×10^{-10}	12	98
	CF_3COOH	2.9×10^{4}	1.9×10^{-10} [b]	5.4×10^{-6} [b]	6.1×10^{-10}	1.7×10^{-5}	93
15	MeOH	1.7×10^{12}	1.6×10^{-13}	0.27	unknown	unknown	this work
	$(H_2O)_2$	4.0×10^{14}	3.3×10^{-12}	1.3×10^{3}	unknown	unknown	18, 67
	CF_3COOH	2.9×10^{4}	1.9×10^{-10} [b]	5.4×10^{-6} [b]	unknown	unknown	93
16	MeOH	1.7×10^{12}	5.1×10^{-13}	0.87	unknown	unknown	this work
	$(H_2O)_2$	4.0×10^{14}	2.2×10^{-11}	8.8×10^{3}	unknown	unknown	2, 5

[a]Where available, computed rate constants [k_{eff}(th)] with experimental values [k_{eff}(ex)]. Tropospheric concentrations and experimental rate constants are taken from the references shown in the final column. [b]*Reaction rate constants based upon previously reported* ΔG_{TS} *all exceed the computed gas collision limit, and so only this collision limit is reported here.*

all exceed the gas collision limit as shown at Supporting Information Table S2.

Although there is a trend between electronic character and reactivity, there are exceptions, where steric repulsion from bulky substituents prevents access to the carbonyl oxide moiety. Orr-Ewing and co-workers demonstrated that the reaction of methanol with $(CH_3)_2COO$ ($k_{(T=292.6K,\ P=9.99\ Torr)}$ = 4.29×10^{-14} cm^3 molec^{-1} s^{-1}) is significantly slower than the reaction of methanol with CH_2OO ($k_{(T=292.6\ K,\ P=9.99\ Torr)}$ = 1.04×10^{-13} cm^3 molec^{-1} s^{-1}).[39] Here it is demonstrated that the $(CH_3)_2COO$ bimolecular reaction coordinate has a positive reaction barrier, whereas the CH_2OO bimolecular reaction has a somewhat less stable prereaction complex but has low-energy transition state. These changes to the potential energy surfaces are analogous to those discussed in the previous section pertaining to *syn*-/*anti*-CH_3CHOO and can be attributed to the methyl groups creating steric hindrance to nucleophilic attack that offsets the greater zwitterionic character of $(CH_3)_2COO$ (R_{OO}/R_{CO} = 1.091) compared to CH_2OO (R_{OO}/R_{CO} = 1.078).

IV. VHP Channel and the Effect of Tunneling. Stabilized Criegee intermediates **2**, **4**, **13**, and **14** all possess an α-methyl group relative to the terminal oxygen and therefore can undergo a 1,4-hydrogen shift mechanism leading to unimolecular decomposition. The transition state in these reactions is characterized by light atom (H atom) motion, and as such, it is anticipated that tunneling could facilitate increased unimolecular decomposition rates. Further, previous studies have shown that hydroxyl-containing species, such as H_2O, may catalyze this unimolecular decomposition, by reducing the energetic cost of the 1,4-hydrogen transfer processes leading to production of alkyl hydroperoxides.[21,22] Although the uncatalyzed reactions typically exhibit slow reaction rates at room temperature, these catalytic pathways may become competitive with bimolecular reaction pathways, as in the case of the water-catalyzed reactions, where branching ratios (Γ) to this decomposition channel are as high as 0.13.

DOI: 10.1021/acs.jpca.8b09349
J. Phys. Chem. A 2019, 123, 218−229

Analogous methanol-catalyzed unimolecular channels (Figure 2) were identified in this work. In each case [**2**, **4**, **13**, and **14**] a low-energy decomposition pathway exists, where a 1,4-H shift leads to the formation of a VHP, which may then undergo subsequent O−O bond fission to form an OH radical and an alkoxy radical.[7,69−71] The transition states for these catalytic channels are dominated by concerted hydrogen shifts between the sCI and the alcohol, again leading to the assertion that tunneling may increase observed reaction rates. Where these channels exist, they are reported in Table 2.

To investigate the effects of catalyzed unimolecular decomposition, tunneling constants are computed using an asymmetric Eckart function treatment that takes into account the potential energy barrier width, unlike a more simplistic Wigner approach, which accounts only for the magnitude of the imaginary frequency of the transition state. The validity of this methodology is tested against two Criegee intermediate test cases, namely, the tunneling contributions for uncatalyzed unimolecular decomposition of **CI 2** and **CI 14**, at multiple temperatures. For each system, tunneling factors are evaluated using a simplistic Wigner approach, the Eckart function treatment, and a more complex and accurate instanton-based approach.

Briefly, implemented in the MOLPRO computational suite, the semiclassical on-the-fly instanton method proceeds by optimizing the structure of a ring-polymer bead potential, which is described by a number of N beads that straddle the transition state, coupled by an effective harmonic potential.[54] These "beads" are simply geometries close to the transition state path. The instanton path, that is, the path of least action, is found by optimizing this potential for an increasing number of beads. As $N \rightarrow \infty$, the Eyring and instanton rate equations approach their exact values, at the cost of increasing the computational expense of the calculation. The optimized bead potential can then be used to calculate the action of the instanton path (the tunneling constant) and estimate the reaction rate constant, inclusive of tunneling. This methodology, coupled with high-level electronic structure theory, can be expected to capture accurate estimates of the tunneling enhancement of reaction rate, but it is not suitable for extensions to the larger molecular systems due to the computational cost. Here, calculations were performed using DF-DFT//B3LYP/cc-pVTZ and CCSD(T)/cc-pVTZ levels of theory. For more details, the reader is referred to refs 72−76.

As expected, both the Eckart function methodology and the instanton approach appear to provide a much more reasonable description of the tunneling factor than the simplistic Wigner approach, consistent with those reported for water-catalyzed reactions. The similarity of the Eckart and instanton tunneling factors, with discrepancies of less than 1 order of magnitude, demonstrates that the Eckart approach is suitable for use in Criegee intermediate systems. Including tunneling contributions to catalyzed unimolecular decomposition, the total branching ratio (Γ) for the VHP channel still only reaches 0.057 in the case of **CI 2**. For sCIs **4**, **13**, and **14**, the VHP branching ratio is less than 0.011, again despite large tunneling constants ($\kappa_{\mathrm{CI13\ VHP\ channel\ 1}} = 94.79$), illustrating that the alcohol-catalyzed unimolecular decomposition is relatively unimportant for all sCI−alcohol reactions. The Eckart tunneling constant has also been computed for all bimolecular AAAH channels, giving values ranging from 1 to 2.44, predominantly due to the mixed heavy atom motion at the transition states for these channels, which, as anticipated, prevents significant tunneling contributions. In the case of $(CH_3)_2COO$, the computed VHP channel branching ratio is 0.010, with almost no tunneling contribution to the bimolecular reaction channel ($\kappa_{\mathrm{Eckart}} = 1.35$). These results are consistent with experimental measurements that show little change in the reaction rate of $(CH_3)_2COO$ with methanol, upon alcohol deuteration, at 282.5 K < T < 328.5 K.[39]

Of the reactions studied, only the reaction of *syn*-CH_3CHOO with methanol shows a competitive unimolecular decomposition channel, mainly due to the low-energy barrier for this hydrogen shift pathway, rather than an exceptionally high tunneling constant.

V. Atmospheric Implications. Table 3 shows the effective rate constants (k_{eff}) of the sCI−alcohol reactions, in comparison to other trace atmospheric species, using concentrations found in Sao Paulo (atmospheric humidity ∼80%). In each case, the coreactant in eq 11 is an alcohol, with concentrations of 34.1, 176.3, and 44.2 ppbv for methanol, ethanol, and isopropyl alcohol, respectively.[77]

To consider the atmospheric implications of these results, sCI−alcohol reaction rates should be considered at both a local and global level. On a global level, sCI bimolecular reactions with water vapor, bimolecular reaction with trace tropospheric species, and unimolecular decomposition are more significant loss processes for Criegee intermediates due to low alcohol abundances. Despite this, Orr-Ewing and co-workers suggest that in those local areas where alcohol and alkene emissions are both high, for example, in rainforests, sCI−alcohol reactions may be a significant source of AAAHs (∼30 Gg yr^{-1})[39]

In standard urban environments, such as Osaka in Japan, methanol, ethanol, and isopropyl alcohol concentrations are typically ca. 5−10 ppbv, such that sCI−alcohol reactions are again not competitive with other sCI reactions with tropospheric pollutants, like SO_2/NO_2. Organic and inorganic acid reactions with sCIs are competitive with OH radicals, as demonstrated by the review by Khan and co-workers.[99] However, in cities where biofuel use is prevalent, both tropospheric alcohol and ozone concentrations are increased.[100] The effective rate of reaction (k_{eff}) is therefore also evaluated using the alcohol concentrations of Sao Paulo, Brazil ([MeOH] = 34.1 ppbv, [EtOH] = 176.3 ppbv and [iPrOH] = 44.2 ppbv).[11] Under these tropospheric conditions, sCI−alcohol reactions begin to compete with, but still do not dominate, sCI removal, which are still predominantly lost through reaction with water or water dimer, regardless of sCI size or complexity.[101] However, the increased k_{eff} under these conditions again suggests that sCI−alcohol reactions should be a significant source of AAAH's and that AAAH concentrations may well be elevated in these urban environments, where biofuel use is prevalent.

VI. Conclusion. High-level, ab initio computational chemistry has been utilized to analyze the bimolecular gas-phase reactions of 22 different stabilized Criegee intermediates with common tropospheric alcohols. These sCI−alcohol reactions follow one of two major channels: the dominant channel proceeds through a prereaction complex and then traverses a low-lying transition state leading to the formation of AAAHs. The second channel is an alcohol-catalyzed unimolecular decomposition of sCIs into vinyl hydroperoxides. This second channel is only accessible to sCIs with an α-methyl group.

In the first pathway, accessible to all sCIs, substitution of the alcohol coreactant has little influence on the reaction rate.

DOI: 10.1021/acs.jpca.8b09349
J. Phys. Chem. A 2019, 123, 218−229

Comparison between theoretical and experimental rate constants for the reaction of CH_2OO with methanol, ethanol, and isopropyl alcohol show good agreement, with the computational results matching the experimentally observed trend in reactivity (methanol > isopropyl alcohol > ethanol). The agreement between theory and experiment is even more remarkable when comparing the temperature dependence of these reactions. The computational potential energy surfaces generated in this work lead to reaction kinetics that clearly reproduce the negative temperature dependences of the reactions of CH_2OO with methanol and ethanol and also illustrate the mixed temperature dependence of $(CH_3)_2COO$ with methanol. This latter reaction can only be modeled accurately by considering the multiple low-lying reactive transition states.

In all of the reactions studied in this report, it is the barrier height of the lowest transition state that dominates the reaction kinetics, and the barrier height can be attributed to several different factors. Steric bulkiness of the sCI substituents leads to a reduction in sCI−alcohol reaction rate, and the more electronegative the sCI substituents, or more conjugated, the zwitterionic character of the carbonyl oxide moiety increases, which leads to an increase in in sCI−alcohol reaction rate. In monosubstituted sCIs, the differences in conformeric forms also influences reaction rate, with *anti*-sCIs often exhibiting several orders of magnitude increased reaction rates.

The second reaction channel is an alcohol-catalyzed sCI decomposition pathway. Analysis of this pathway shows that the mechanism proceeds through transition states dominated by light atom motion, leading to significant tunneling contributions to the reaction rates at room temperature. However, the branching ratio for this channel never exceeds 0.067 even where tunneling is important and in reactive systems where multiple decomposition pathways exist. This is therefore a very insignificant atmospheric reaction channel.

■ ASSOCIATED CONTENT

Supporting Information

The Supporting Information is available free of charge on the ACS Publications website at DOI: 10.1021/acs.jpca.8b09349.

A sensitivity study comparing experimental rate constants with computational rate constants using Gibbs free energy; computed gas collision limits; a full breakdown of rate constants for sCIs 1−22 with MeOH and sCIs 1,11 and 12 with EtOH and iPrOH; relative energies [kJ mol^{-1}] of stationary points for sCI reactions with alcohols; a full breakdown of rate constants for reactions of CH_2OO + MeOH, CH_2OO + EtOH, and $(CH_3)_2COO$ + MeOH through temperature range of 200 K < T < 500 K at p = 760 Torr; a full breakdown of rate constants of reactions CH_2OO + MeOH, CH_2OO + EtOH, and $(CH_3)_2COO$ + MeOH through temperature range of 200 K < T < 350 K at p = 9.99 Torr; calculated values for CI + ROH rate constants at selected temperatures and pressures for direct comparison with experiment; Cartesian coordinates of all stationary points, and IRCs of all transition states in this study (PDF)

■ AUTHOR INFORMATION

Corresponding Author

*E-mail: beamesj@cardiff.ac.uk.

ORCID

Peter J. Knowles: 0000-0003-4657-6331

Joseph M. Beames: 0000-0002-5508-8236

Present Address

[†]Dr. Joshua A. Black, Institut für Theoretische Chemie, Universität Stuttgart, Pfaffenwaldring 55, 70569 Stuttgart, Germany.

Author Contributions

The manuscript was written through contributions of all authors. All authors have given approval to the final version of the manuscript.

Notes

The authors declare no competing financial interest.

■ ACKNOWLEDGMENTS

This work was partially supported by Advanced Research Computing at Cardiff and High Performance Computing Wales, a company formed between the universities and the private sector in Wales, which provides the U.K.'s largest distributed supercomputing network. We thank the EPSRC for DTP studentship funding for TS and JB (grants EP/M507842/1, EP/P505453/1, EP/J500197/1 and EP/K502819/1). Dr. J. M. Beames is supported through Marie Skłodowska Curie Individual Fellowship NPTC (701593). Information on the data underpinning the results presented here is shown in the Supplementary Information.

■ ABBREVIATIONS

sCI, stabilized Criegee intermediate; AAAHs, α-alkoxyalkyl hydroperoxides; VHP, vinylhydroperoxide

■ REFERENCES

(1) Docherty, K. S.; Ziemann, P. J. Effects of Stabilized Criegee Intermediate and OH Radical Scavengers on Aerosol Formation from Reactions of β-Pinene with O_3. *Aerosol Sci. Technol.* **2003**, *37* (11), 877−891.

(2) Womack, C. C.; Martin-Drumel, M.-A.; Brown, G. G.; Field, R. W.; McCarthy, M. C. Observation of the Simplest Criegee Intermediate CH_2OO in the Gas-Phase Ozonolysis of Ethylene. *Sci. Adv.* **2015**, *1* (2), No. e1400105.

(3) Welz, O.; Savee, J. D.; Osborn, D. L.; Vasu, S. S.; Percival, C. J.; Shallcross, D. E.; Taatjes, C. A. Direct Kinetic Measurements of Criegee Intermediate (CH_2OO) Formed by Reaction of CH_2I with O_2. *Science* **2012**, *335* (6065), 204−207.

(4) Asatryan, R.; Bozzelli, J. W. Formation of a Criegee Intermediate in the Low-Temperature Oxidation of Dimethyl Sulfoxide. *Phys. Chem. Chem. Phys.* **2008**, *10* (13), 1769−1780.

(5) Johnson, D.; Marston, G. The Gas-Phase Ozonolysis of Unsaturated Volatile Organic Compounds in the Troposphere. *Chem. Soc. Rev.* **2008**, *37* (4), 699−716.

(6) Neeb, P.; Horie, O.; Moortgat, G. K. The Ethene−Ozone Reaction in the Gas Phase. *J. Phys. Chem. A* **1998**, *102* (34), 6778−6785.

(7) Martinez, R. I.; Herron, J. T. Stopped-Flow Studies of the Mechanisms of Ozone-Alkene Reactions in the Gas Phase: Trans-2-Butene. *J. Phys. Chem.* **1988**, *92* (16), 4644−4648.

(8) Niki, H.; Maker, P. D.; Savage, C. M.; Breitenbach, L. P.; Hurley, M. D. FTIR Spectroscopic Study of the Mechanism for the Gas-Phase Reaction between Ozone and Tetramethylethylene. *J. Phys. Chem.* **1987**, *91* (4), 941−946.

(9) Cremer, D.; Gauss, J.; Kraka, E.; Stanton, J. F.; Bartlett, R. J. A CCSD (T) Investigation of Carbonyl Oxide and Dioxirane. Equilibrium Geometries, Dipole Moments, Infrared Spectra, Heats of Formation and Isomerization Energies. *Chem. Phys. Lett.* **1993**, *209* (5), 547−556.

(10) Gutbrod, R.; Schindler, R. N.; Kraka, E.; Cremer, D. Formation of OH Radicals in the Gas Phase Ozonolysis of Alkenes: The Unexpected Role of Carbonyl Oxides. *Chem. Phys. Lett.* **1996**, *252* (3), 221−229.
(11) Gutbrod, R.; Kraka, E.; Schindler, R. N.; Cremer, D. Kinetic and Theoretical Investigation of the Gas-Phase Ozonolysis of Isoprene: Carbonyl Oxides as an Important Source for OH Radicals in the Atmosphere. *J. Am. Chem. Soc.* **1997**, *119* (31), 7330−7342.
(12) Horie, O.; Moortgat, G. K. Gas-Phase Ozonolysis of Alkenes. Recent Advances in Mechanistic Investigations. *Acc. Chem. Res.* **1998**, *31* (7), 387−396.
(13) Horie, O.; Moortgat, G. K. Decomposition Pathways of the Excited Criegee Intermediates in the Ozonolysis of Simple Alkenes. *Atmos. Environ., Part A* **1991**, *25* (9), 1881−1896.
(14) Su, F.; Calvert, J. G.; Shaw, J. H. A FT IR Spectroscopic Study of the Ozone-Ethene Reaction Mechanism in Oxygen-Rich Mixtures. *J. Phys. Chem.* **1980**, *84* (3), 239−246.
(15) Atkinson, R. Gas-Phase Tropospheric Chemistry of Volatile Organic Compounds: 1. Alkanes and Alkenes. *J. Phys. Chem. Ref. Data* **1997**, *26* (2), 215−290.
(16) Chhantyal-Pun, R.; Welz, O.; Savee, J. D.; Eskola, A. J.; Lee, E. P. F.; Blacker, L.; Hill, H. R.; Ashcroft, M.; Khan, M. A. H.; Lloyd-Jones, G. C.; et al. Direct Measurements of Unimolecular and Bimolecular Reaction Kinetics of the Criegee Intermediate $(CH_3)_2COO$. *J. Phys. Chem. A* **2017**, *121* (1), 4−15.
(17) Chhantyal-Pun, R.; Davey, A.; Shallcross, D. E.; Percival, C. J.; Orr-Ewing, A. J. A Kinetic Study of the CH_2OO Criegee Intermediate Self-Reaction, Reaction with SO_2 and Unimolecular Reaction Using Cavity Ring-down Spectroscopy. *Phys. Chem. Chem. Phys.* **2015**, *17* (5), 3617−3626.
(18) Huang, H.-L.; Chao, W.; Lin, J. J.-M. Kinetics of a Criegee Intermediate That Would Survive High Humidity and May Oxidize Atmospheric SO_2. *Proc. Natl. Acad. Sci. U. S. A.* **2015**, *112* (35), 10857−10862.
(19) Chao, W.; Hsieh, J.-T.; Chang, C.-H.; Lin, J. J.-M. Direct Kinetic Measurement of the Reaction of the Simplest Criegee Intermediate with Water Vapor. *Science* **2015**, *347* (6223), 751−754.
(20) Kumar, M.; Francisco, J. S. H−X (X = H, CH_3, CH_2F, CHF_2, CF_3, and SiH_3) Bond Activation by Criegee Intermediates: A Theoretical Perspective. *J. Phys. Chem. A* **2017**, *121* (49), 9421−9428.
(21) Anglada, J. M.; Solé, A. Impact of the Water Dimer on the Atmospheric Reactivity of Carbonyl Oxides. *Phys. Chem. Chem. Phys.* **2016**, *18* (26), 17698−17712.
(22) Anglada, J. M.; González, J.; Torrent-Sucarrat, M. Effects of the Substituents on the Reactivity of Carbonyl Oxides. A Theoretical Study on the Reaction of Substituted Carbonyl Oxides with Water. *Phys. Chem. Chem. Phys.* **2011**, *13* (28), 13034−13045.
(23) Zhu, C.; Kumar, M.; Zhong, J.; Li, L.; Francisco, J. S.; Zeng, X. C. New Mechanistic Pathways for Criegee−Water Chemistry at the Air/Water Interface. *J. Am. Chem. Soc.* **2016**, *138* (35), 11164−11169.
(24) Zhong, J.; Kumar, M.; Zhu, C. Q.; Francisco, J. S.; Zeng, X. C. Surprising Stability of Larger Criegee Intermediates on Aqueous Interfaces. *Angew. Chem., Int. Ed.* **2017**, *56* (27), 7740−7744.
(25) Kumar, M.; Zhong, J.; Francisco, J. S.; Zeng, X. C. Criegee Intermediate-Hydrogen Sulfide Chemistry at the Air/Water Interface. *Chem. Sci.* **2017**, *8* (8), 5385−5391.
(26) Zhong, J.; Kumar, M.; Francisco, J. S.; Zeng, X. C. Insight into Chemistry on Cloud/Aerosol Water Surfaces. *Acc. Chem. Res.* **2018**, *51* (5), 1229−1237.
(27) Kumar, M.; Zhong, J.; Zeng, X. C.; Francisco, J. S. Reaction of Criegee Intermediate with Nitric Acid at the Air−Water Interface. *J. Am. Chem. Soc.* **2018**, *140*, 4913.
(28) Kumar, M.; Francisco, J. S. Heteroatom Tuning of Bimolecular Criegee Reactions and Its Implications. *Angew. Chem., Int. Ed.* **2016**, *55* (43), 13432−13435.
(29) Murphy, K. V.; Morgan, W. J.; Sun, Z.; Schaefer, H. F.; Agarwal, J. Thioformaldehyde S-Sulfide, Sulfur Analogue of the Criegee Intermediate: Structures, Energetics, and Rovibrational Analysis. *J. Phys. Chem. A* **2017**, *121* (5), 998−1006.
(30) Trabelsi, T.; Kumar, M.; Francisco, J. S. How Does the Central Atom Substitution Impact the Properties of a Criegee Intermediate? Insights from Multireference Calculations. *J. Am. Chem. Soc.* **2017**, *139* (43), 15446−15449.
(31) Novelli, A.; Hens, K.; Tatum-Ernest, C.; Martinez, M.; Nolscher, A.; Sinha, V.; Paasonen, P.; Petaja, T.; Sipila, M.; Elste, T.; et al. Estimating the Atmospheric Concentration of Criegee Intermediates and Their Possible Interference in a FAGE-LIF Instrument. *Atmos. Chem. Phys.* **2017**, *17*, 7807−7826.
(32) Grosjean, E.; Rasmussen, R. A.; Grosjean, D. Ambient Levels of Gas Phase Pollutants in Porto Alegre, Brazil. *Atmos. Environ.* **1998**, *32* (20), 3371−3379.
(33) Kelly, T. J.; Callahan, P. J.; Pleil, J.; Evans, G. F. Method Development and Field Measurements for Polar Volatile Organic Compounds in Ambient Air. *Environ. Sci. Technol.* **1993**, *27* (6), 1146−1153.
(34) Grosjean, E.; Grosjean, D.; Gunawardena, R.; Rasmussen, R. A. Ambient Concentrations of Ethanol and Methyl Tert-Butyl Ether in Porto Alegre, Brazil, March 1996−April 1997. *Environ. Sci. Technol.* **1998**, *32* (6), 736−742.
(35) de Paula Pereira, P. A.; Sousa Santos, E. T.; de Freitas Ferreira, T.; de Andrade, J. B. Determination of Methanol and Ethanol by Gas Chromatrography Following Air Sampling onto Florisil Cartridges and Their Concentrations at Urban Sites in the Three Largest Cities in Brazil. *Talanta* **1999**, *49* (2), 245−252.
(36) Colón, M.; Pleil, J. D.; Hartlage, T. A.; Lucia Guardani, M.; Helena Martins, M. Survey of Volatile Organic Compounds Associated with Automotive Emissions in the Urban Airshed of São Paulo, Brazil. *Atmos. Environ.* **2001**, *35* (23), 4017−4031.
(37) Salvo, A.; Geiger, F. M. Reduction in Local Ozone Levels in Urban São Paulo Due to a Shift from Ethanol to Gasoline Use. *Nat. Geosci.* **2014**, *7* (6), 450−458.
(38) Gäb, S.; Hellpointner, E.; Turner, W. V.; Koŕte, F. Hydroxymethyl Hydroperoxide and Bis(Hydroxymethyl) Peroxide from Gas-Phase Ozonolysis of Naturally Occurring Alkenes. *Nature* **1985**, *316* (6028), 535−536.
(39) McGillen, M. R.; Curchod, B. F. E.; Chhantyal-Pun, R.; Beames, J. M.; Watson, N.; Khan, M. A. H.; McMahon, L.; Shallcross, D. E.; Orr-Ewing, A. J. Criegee Intermediate−Alcohol Reactions, A Potential Source of Functionalized Hydroperoxides in the Atmosphere. *ACS Earth Space Chem.* **2017**, *1* (10), 664−672.
(40) Tadayon, S. V.; Foreman, E. S.; Murray, C. Kinetics of the Reactions between the Criegee Intermediate CH_2OO and Alcohols. *J. Phys. Chem. A* **2018**, *122* (1), 258−268.
(41) Neeb, P.; Horie, O.; Moortgat, G. Gas-Phase Ozonolysis of Ethene in the Presence of Hydroxylic Compounds. *Int. J. Chem. Kinet.* **1996**, *28*, 721−730.
(42) Tobias, H. J.; Ziemann, P. J. Kinetics of the Gas-Phase Reactions of Alcohols, Aldehydes, Carboxylic Acids, and Water with the C13 Stabilized Criegee Intermediate Formed from Ozonolysis of 1-Tetradecene. *J. Phys. Chem. A* **2001**, *105* (25), 6129−6135.
(43) Lin, Y.-H.; Takahashi, K.; Lin, J. J.-M. Reactivity of Criegee Intermediates toward Carbon Dioxide. *J. Phys. Chem. Lett.* **2018**, *9* (1), 184−188.
(44) Kumar, M.; Busch, D. H.; Subramaniam, B.; Thompson, W. H. Criegee Intermediate Reaction with CO: Mechanism, Barriers, Conformer-Dependence, and Implications for Ozonolysis Chemistry. *J. Phys. Chem. A* **2014**, *118* (10), 1887−1894.
(45) Xu, K.; Wang, W.; Wei, W.; Feng, W.; Sun, Q.; Li, P. Insights into the Reaction Mechanism of Criegee Intermediate CH_2OO with Methane and Implications for the Formation of Methanol. *J. Phys. Chem. A* **2017**, *121* (38), 7236−7245.
(46) Lee, C.; Yang, W.; Parr, R. G. Development of the Colle-Salvetti Correlation-Energy Formula into a Functional of the Electron Density. *Phys. Rev. B: Condens. Matter Mater. Phys.* **1988**, *37* (2), 785−789.
(47) Kendall, R. A.; Dunning, T. H.; Harrison, R. J. Electron Affinities of the First-row Atoms Revisited. Systematic Basis Sets and Wave Functions. *J. Chem. Phys.* **1992**, *96* (9), 6796−6806.

DOI: 10.1021/acs.jpca.8b09349
J. Phys. Chem. A 2019, 123, 218−229

(48) Becke, A. D. Density-functional Thermochemistry. III. The Role of Exact Exchange. *J. Chem. Phys.* **1993**, *98* (7), 5648−5652.
(49) Dunning, T. H. Gaussian Basis Sets for Use in Correlated Molecular Calculations. I. The Atoms Boron through Neon and Hydrogen. *J. Chem. Phys.* **1989**, *90* (2), 1007−1023.
(50) Gonzalez, C.; Schlegel, H. B. Reaction Path Following in Mass-Weighted Internal Coordinates. *J. Phys. Chem.* **1990**, *94* (14), 5523−5527.
(51) Ishida, K.; Morokuma, K.; Komornicki, A. The Intrinsic Reaction Coordinate. An *ab initio* Calculation for HNC→HCN and $H^- + CH_4 \rightarrow CH_4 + H^-$. *J. Chem. Phys.* **1977**, *66* (5), 2153−2156.
(52) Frisch, M. J.; Trucks, G. W.; Schlegel, H. B.; Scuseria, G. E.; Robb, M. A.; Cheeseman, J. R.; Scalmani, G.; Barone, V.; Petersson, G. A.; Nakatsuji, H.; et al. *Gaussian 09,* Revision A.02; Gaussian, Inc: Wallingford, CT, 2016.
(53) Adler, T. B.; Werner, H.-J. An Explicitly Correlated Local Coupled Cluster Method for Calculations of Large Molecules Close to the Basis Set Limit. *J. Chem. Phys.* **2011**, *135* (14), 144117.
(54) Werner, H.-J.; Knowles, P. J.; Knizia, G.; Manby, F. R.; Schütz, M. Molpro: A General-Purpose Quantum Chemistry Program Package: Molpro. *WIREs Comput. Mol. Sci.* **2012**, *2* (2), 242−253.
(55) Canneaux, S.; Bohr, F.; Henon, E. KiSThelP: A Program to Predict Thermodynamic Properties and Rate Constants from Quantum Chemistry Results. *J. Comput. Chem.* **2014**, *35* (1), 82−93.
(56) Zhao, Q.; Liu, F.; Wang, W.; Li, C.; Lü, J.; Wang, W. Reactions between Hydroxyl-Substituted Alkylperoxy Radicals and Criegee Intermediates: Correlations of the Electronic Characteristics of Methyl Substituents and the Reactivity. *Phys. Chem. Chem. Phys.* **2017**, *19* (23), 15073−15083.
(57) Kumar, M.; Francisco, J. S. Reactions of Criegee Intermediates with Non-Water Greenhouse Gases: Implications for Metal Free Chemical Fixation of Carbon Dioxide. *J. Phys. Chem. Lett.* **2017**, *8* (17), 4206−4213.
(58) Shiroudi, A.; Deleuze, M. S.; Canneaux, S. Theoretical Study of the Oxidation Mechanisms of Naphthalene Initiated by Hydroxyl Radicals: The OH-Addition Pathway. *J. Phys. Chem. A* **2014**, *118* (26), 4593−4610.
(59) Zeng, Z.; Altarawneh, M.; Oluwoye, I.; Glarborg, P.; Dlugogorski, B. Z. Inhibition and Promotion of Pyrolysis by Hydrogen Sulfide (H_2S) and Sulfanyl Radical (SH). *J. Phys. Chem. A* **2016**, *120* (45), 8941−8948.
(60) Wang, Q.-D.; Liu, Z.-W. Reaction Kinetics of Hydrogen Atom Abstraction from C4−C6 Alkenes by the Hydrogen Atom and Methyl Radical. *J. Phys. Chem. A* **2018**, *122* (23), 5202−5210.
(61) Oliaey, A. R.; Shiroudi, A.; Zahedi, E.; Deleuze, M. S. Theoretical Study on the Mechanisms and Kinetics of the β-Elimination of 2,2-Dihaloethyltrihalosilanes (X = F, Cl, Br) Compounds: A DFT Study along with a Natural Bond Orbital Analysis. *React. Kinet., Mech. Catal.* **2018**, *124* (1), 27−44.
(62) Borbon, A.; Gilman, J. B.; Kuster, W. C.; Grand, N.; Chevaillier, S.; Colomb, A.; Dolgorouky, C.; Gros, V.; Lopez, M.; Sarda-Esteve, R.; et al. Emission Ratios of Anthropogenic Volatile Organic Compounds in Northern Mid-Latitude Megacities: Observations versus Emission Inventories in Los Angeles and Paris. *J. Geophys Res. Atmos* **2013**, *118* (4), 2041−2057.
(63) H. Khan, M. A.; Percival, C. J.; Shallcross, D. E.; A. Shallcross, B. M.; Morris, W. C.; Galloway, M. An Estimation of the Levels of Stabilized Criegee Intermediates in the UK Urban and Rural Atmosphere Using the Steady-State Approximation and the Potential Effects of These Intermediates on Tropospheric Oxidation Cycles. *Int. J. Chem. Kinet.* **2017**, *49* (8), 611−621.
(64) Cabezas, C.; Guillemin, J.-C.; Endo, Y. Conformational Analysis of Ethyl-Substituted Criegee Intermediate by FTMW Spectroscopy. *J. Chem. Phys.* **2016**, *145* (22), 224314.
(65) Liu, F.; Beames, J. M.; Green, A. M.; Lester, M. I. UV Spectroscopic Characterization of Dimethyl- and Ethyl-Substituted Carbonyl Oxides. *J. Phys. Chem. A* **2014**, *118* (12), 2298−2306.
(66) Lin, H.-Y.; Huang, Y.-H.; Wang, X.; Bowman, J. M.; Nishimura, Y.; Witek, H. A.; Lee, Y.-P. Infrared Identification of the Criegee Intermediates *Syn*- and *Anti*-CH_3CHOO, and Their Distinct Conformation-Dependent Reactivity. *Nat. Commun.* **2015**, *6*, 7012.
(67) Taatjes, C. A.; Meloni, G.; Selby, T. M.; Trevitt, A. J.; Osborn, D. L.; Percival, C. J.; Shallcross, D. E. Direct Observation of the Gas-Phase Criegee Intermediate (CH_2OO). *J. Am. Chem. Soc.* **2008**, *130* (36), 11883−11885.
(68) Taatjes, C. A.; Welz, O.; Eskola, A. J.; Savee, J. D.; Scheer, A. M.; Shallcross, D. E.; Rotavera, B.; Lee, E. P. F.; Dyke, J. M.; Mok, D. K. W.; et al. Direct Measurements of Conformer-Dependent Reactivity of the Criegee Intermediate CH_3CHOO. *Science* **2013**, *340* (6129), 177−180.
(69) Martinez, R. I.; Herron, J. T. Stopped-Flow Studies of the Mechanisms of Ozone-Alkene Reactions in the Gas Phase: Tetramethylethylene. *J. Phys. Chem.* **1987**, *91* (4), 946−953.
(70) Kristensen, K.; Watne, Å. K.; Hammes, J.; Lutz, A.; Petäjä, T.; Hallquist, M.; Bilde, M.; Glasius, M. High-Molecular Weight Dimer Esters Are Major Products in Aerosols from α-Pinene Ozonolysis and the Boreal Forest. *Environ. Sci. Technol. Lett.* **2016**, *3* (8), 280−285.
(71) Herron, J. T.; Huie, R. E. Stopped-flow Studies of the Mechanisms of Ozone−Alkene Reactions in the Gas Phase Propene and Isobutene. *Int. J. Chem. Kinet.* **1978**, *10* (10), 1019−1041.
(72) Beyer, A. N.; Richardson, J. O.; Knowles, P. J.; Rommel, J.; Althorpe, S. C. Quantum Tunneling Rates of Gas-Phase Reactions from On-the-Fly Instanton Calculations. *J. Phys. Chem. Lett.* **2016**, *7* (21), 4374−4379.
(73) Habershon, S.; Manolopoulos, D. E.; Markland, T. E.; Miller, T. F. Ring-Polymer Molecular Dynamics: Quantum Effects in Chemical Dynamics from Classical Trajectories in an Extended Phase Space. *Annu. Rev. Phys. Chem.* **2013**, *64* (1), 387−413.
(74) Richardson, J. O. Derivation of Instanton Rate Theory from First Principles. *J. Chem. Phys.* **2016**, *144* (11), 114106.
(75) Richardson, J. O.; Althorpe, S. C. Ring-Polymer Molecular Dynamics Rate-Theory in the Deep-Tunneling Regime: Connection with Semiclassical Instanton Theory. *J. Chem. Phys.* **2009**, *131* (21), 214106.
(76) Richardson, J. O.; Althorpe, S. C. Ring-Polymer Instanton Method for Calculating Tunneling Splittings. *J. Chem. Phys.* **2011**, *134* (5), 054109.
(77) Nguyen, H. T.-H.; Takenaka, N.; Bandow, H.; Maeda, Y.; de Oliva, S. T.; Botelho, M. M. f.; Tavares, T. M. Atmospheric Alcohols and Aldehydes Concentrations Measured in Osaka, Japan and in Sao Paulo, Brazil. *Atmos. Environ.* **2001**, *35* (18), 3075−3083.
(78) Lin, L.-C.; Chang, H.-T.; Chang, C.-H.; Chao, W.; Smith, M. C.; Chang, C.-H.; Takahashi, K.; et al. Competition between H_2O and $(H_2O)_2$ Reactions with CH_2OO/CH_3CHOO. *Phys. Chem. Chem. Phys.* **2016**, *18* (6), 4557−4568.
(79) Fang, Y.; Liu, F.; Barber, V. P.; Klippenstein, S. J.; McCoy, A. B.; Lester, M. I. Communication: Real Time Observation of Unimolecular Decay of Criegee Intermediates to OH Radical Products. *J. Chem. Phys.* **2016**, *144* (6), 061102.
(80) Vereecken, L.; Rickard, A. R.; Newland, M. J.; Bloss, W. J. Theoretical Study of the Reactions of Criegee Intermediates with Ozone, Alkylhydroperoxides, and Carbon Monoxide. *Phys. Chem. Chem. Phys.* **2015**, *17* (37), 23847−23858.
(81) Bravo, M. A.; Son, J.; de Freitas, C. U.; Gouveia, N.; Bell, M. L. Air Pollution and Mortality in São Paulo, Brazil: Effects of Multiple Pollutants and Analysis of Susceptible Populations. *J. Exposure Sci. Environ. Epidemiol.* **2016**, *26* (2), 150−161.
(82) Chang, Y.-P.; Chang, H.-H.; Lin, J. J.-M. Kinetics of the Simplest Criegee Intermediate Reaction with Ozone Studied by Mid-Infrared Quantum Cascade Laser Spectrometer. *Phys. Chem. Chem. Phys.* **2018**, *20*, 97−102.
(83) Kuwata, K. T.; Guinn, E. J.; Hermes, M. R.; Fernandez, J. A.; Mathison, J. M.; Huang, K. A Computational Re-Examination of the Criegee Intermediate−Sulfur Dioxide Reaction. *J. Phys. Chem. A* **2015**, *119* (41), 10316−10335.
(84) Liu, Y.; Liu, F.; Liu, S.; Dai, D.; Dong, W.; Yang, X. A Kinetic Study of the CH2OO Criegee Intermediate Reaction with SO_2,

DOI: 10.1021/acs.jpca.8b09349
J. Phys. Chem. A 2019, 123, 218−229

$(H_2O)_2$, CH_2I_2 and I Atoms Using OH Laser Induced Fluorescence. *Phys. Chem. Chem. Phys.* **2017**, *19* (31), 20786−20794.
(85) Vereecken, L.; Nguyen, H. M. T. Theoretical Study of the Reaction of Carbonyl Oxide with Nitrogen Dioxide: $CH_2OO + NO_2$. *Int. J. Chem. Kinet.* **2017**, *49* (10), 752−760.
(86) US Department of Commerce, N. ESRL Global Monitoring Division - Global Greenhouse Gas Reference Network https://www.esrl.noaa.gov/gmd/ccgg/trends/ (accessed Mar 31, 2018).
(87) Raghunath, P.; Lee, Y.-P.; Lin, M. C. Computational Chemical Kinetics for the Reaction of Criegee Intermediate CH_2OO with HNO_3 and Its Catalytic Conversion to OH and HCO. *J. Phys. Chem. A* **2017**, *121* (20), 3871−3878.
(88) Foreman, E. S.; Kapnas, K. M.; Murray, C. Reactions between Criegee Intermediates and the Inorganic Acids HCl and HNO_3: Kinetics and Atmospheric Implications. *Angew. Chem., Int. Ed.* **2016**, *55* (35), 10419−10422.
(89) Crisp, T. A.; Lerner, B. M.; Williams, E. J.; Quinn, P. K.; Bates, T. S.; Bertram, T. H. Observations of Gas Phase Hydrochloric Acid in the Polluted Marine Boundary Layer. *J. Geophys Res. Atmos* **2014**, *119* (11), 6897−6915.
(90) Welz, O.; Eskola, A. J.; Sheps, L.; Rotavera, B.; Savee, J. D.; Scheer, A. M.; Osborn, D. L.; Lowe, D.; Murray Booth, A.; Xiao, P.; et al. Rate Coefficients of C1 and C2 Criegee Intermediate Reactions with Formic and Acetic Acid Near the Collision Limit: Direct Kinetics Measurements and Atmospheric Implications. *Angew. Chem., Int. Ed.* **2014**, *53* (18), 4547−4550.
(91) Bannan, T. J.; Booth, A. M.; Le Breton, M.; Bacak, A.; Muller, J. B. A.; Leather, K. E.; Khan, M. A. H.; Lee, J. D.; Dunmore, R. E.; Hopkins, J. R.; et al. Seasonality of Formic Acid (HCOOH) in London during the ClearfLo Campaign. *J. Geophys Res. Atmos* **2017**, *122* (22), 12488−12498.
(92) Khan, M. A. H.; Lyons, K.; Chhantyal-Pun, R.; McGillen, M. R.; Caravan, R. L.; Taatjes, C. A.; Orr-Ewing, A. J.; Percival, C. J.; Shallcross, D. E. Investigating the Tropospheric Chemistry of Acetic Acid Using the Global 3-D Chemistry Transport Model, STOCHEM-CRI. *J. Geophys Res. Atmos* **2018**, *123* (11), 6267−6281.
(93) Chhantyal-Pun, R.; McGillen, M. R.; Beames, J. M.; Khan, M. A. H.; Percival, C. J.; Shallcross, D. E.; Orr-Ewing, A. J. Temperature-Dependence of the Rates of Reaction of Trifluoroacetic Acid with Criegee Intermediates. *Angew. Chem., Int. Ed.* **2017**, *56* (31), 9044−9047.
(94) Zhang, B.; Zhai, Z.; Zhang, J. Distribution of Trifluoroacetic Acid in Gas and Particulate Phases in Beijing from 2013 to 2016. *Sci. Total Environ.* **2018**, *634*, 471−477.
(95) Vereecken, L. The Reaction of Criegee Intermediates with Acids and Enols. *Phys. Chem. Chem. Phys.* **2017**, *19* (42), 28630−28640.
(96) Lin, L.-C.; Chao, W.; Chang, C.-H.; Takahashi, K.; Lin, J. J.-M. Temperature Dependence of the Reaction of *Anti*-CH_3CHOO with Water Vapor. *Phys. Chem. Chem. Phys.* **2016**, *18* (40), 28189−28197.
(97) Kurtén, T.; Lane, J. R.; Jørgensen, S.; Kjaergaard, H. G. A Computational Study of the Oxidation of SO_2 to SO_3 by Gas-Phase Organic Oxidants. *J. Phys. Chem. A* **2011**, *115* (31), 8669−8681.
(98) Chhantyal-Pun, R.; Rotavera, B.; McGillen, M. R.; Khan, M. A. H.; Eskola, A. J.; Caravan, R. L.; Blacker, L.; Tew, D. P.; Osborn, D. L.; Percival, C. J.; et al. Criegee Intermediate Reactions with Carboxylic Acids: A Potential Source of Secondary Organic Aerosol in the Atmosphere. *ACS Earth Space Chem.* **2018**, *2* (8), 833−842.
(99) Khan, M. A. H.; Percival, C. J.; Caravan, R. L.; Taatjes, C. A.; Shallcross, D. E. Criegee Intermediates and Their Impacts on the Troposphere. *Environ. Sci.: Processes Impacts* **2018**, *20*, 437.
(100) Madronich, S. Atmospheric Chemistry: Ethanol and Ozone. *Nat. Geosci.* **2014**, *7* (6), 395−397.
(101) Monod, A.; Bonnefoy, N.; Kaluzny, P.; Denis, I.; Foster, P.; Carlier, P. Methods for Sampling and Analysis of Tropospheric Ethanol in Gaseous and Aqueous Phases. *Chemosphere* **2003**, *52* (8), 1307−1319.

DOI: 10.1021/acs.jpca.8b09349
J. Phys. Chem. A 2019, 123, 218−229